AD-A256 840

PL-TR-92-2169
ENVIRONMENTAL RESEARCH PAPERS, NO. 1103

OCT 1992

REFINEMENT AND TESTING OF THE RADIATIVE TRANSFER PARAMETERIZATION IN THE PL GLOBAL SPECTRAL MODEL

John L. Schattel, Capt, USAF

18 June 1992

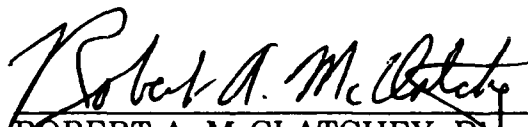**APPROVED FOR PUBLIC RELEASE; DISTRIBUTION UNLIMITED**

92 10 2 030

92-26385

PHILLIPS LABORATORY
Directorate of Geophysics
AIR FORCE SYSTEMS COMMAND
HANSCOM AIR FORCE BASE, MA 01731-5000

"This technical report has been reviewed and is approved for publication"

FOR THE COMMANDER

DONALD A. CHISHOLM, Chief
Atmospheric Prediction Branch

ROBERT A. McCLATCHEY, Director
Atmospheric Sciences Division

REPORT DOCUMENTATION PAGE

Public reporting burden for this collection of information is estimated to average 1 hour per response, including the time for reviewing instructions, searching existing data sources, gathering and maintaining the data needed, and completing and reviewing the collection of information. Send comments regarding this burden estimate or any other aspect of this collection of information, including suggestions for reducing this burden, to Washington Headquarters Services, Directorate for Information Operations and Reports, 1215 Jefferson Davis Highway, Suite 1204, Arlington, VA 22202-4302, and to the Office of Management and Budget, Paperwork Reduction Project (0704-0188), Washington, DC 20503.

1. AGENCY USE ONLY (Leave blank)	2. REPORT DATE 18 June 1992	3. REPORT TYPE AND DATES COVERED Scientific Interim

4. TITLE AND SUBTITLE	5. FUNDING NUMBERS
Refinement and Testing of the Radiative Transfer Parameterization in the PL Global Spectral Model	PE: 62101F PR: 6670 TA: 10 WU: 28
6. AUTHOR(S) John L. Schattel, Captain, USAF	

7. PERFORMING ORGANIZATION NAME(S) AND ADDRESS(ES) Phillips Laboratory (GPAP) Hanscom Air Force Base Massachusetts 01731-5000	8. PERFORMING ORGANIZATION REPORT NUMBER PL-TR-92-2169 ERP, No. 1103

9. SPONSORING MONITORING AGENCY NAME(S) AND ADDRESS(ES)	10. SPONSORING MONITORING AGENCY REPORT NUMBER

11. SUPPLEMENTARY NOTES

12a. DISTRIBUTION AVAILABILITY STATEMENT Approved for public release; distribution unlimited	12b. DISTRIBUTION CODE

13. ABSTRACT (Maximum 200 words) As part of a larger initiative to develop a research-grade advanced physics global spectral numerical weather prediction model, an atmospheric radiative transfer parameterization scheme that interacts with model clouds has been developed. It has been incorporated into the Phillips Laboratory (PL) global spectral model along with state-of-the-art schemes to account for boundary layer exchange process, cumulus convection and gravity wave drag. The radiation scheme employs a broadband approach to account for longwave and shortwave fluxes in clear and cloudy atmospheres. The clear column scheme includes absorption by water vapor, carbon dioxide and ozone. For cloud regions, up to three cloud decks can be handled, corresponding to low, middle, and high clouds. Several procedures to transform the model's distribution of relative humidity at each gridpoint to the three deck cloud solution were evaluated. A variation of the so-called Slingo scheme employed in the global model of the European Centre of Medium-range Weather Forecasting was selected. The radiation flux calculations proceed with one of seven possible cloud layer scenarios and using maximum overlap assumptions. Global model experiments with the cloud-radiation scheme confirmed the successful simulation of observed outgoing longwave radiation (from satellite observations) both in its magnitude and in the proper placement geographically of extrema. Improvements in the global model heating rate profiles resulted, in turn, in improved temperature forecasts throughout the model troposphere/stratosphere.

14. SUBJECT TERMS	15. NUMBER OF PAGES 34
Radiative transfer/Cloud-radiation interactions/Simulation Broadband models/Cloud schemes/Numerical weather prediction	16. PRICE CODE

17. SECURITY CLASSIFICATION OF REPORT	18. SECURITY CLASSIFICATION OF THIS PAGE	19. SECURITY CLASSIFICATION OF ABSTRACT	20. LIMITATION OF ABSTRACT
Unclassified	Unclassified	Unclassified	SAR

Contents

iii

A-1

Illustrations

v

Tables

Refinement and Testing of the Radiative Transfer Parameterization in the PL Global Spectral Model

1. INTRODUCTION

This report documents the Phillips Laboratory (PL) Atmospheric Prediction Branch's effort to integrate an atmospheric radiative transfer parameterization into a Global Spectral Model (GSM). This work is part of a larger initiative, to develop an advanced physics GSM. The advanced physics GSM improves the forecast of various meteorological variables by incorporating parameterizations of the planetary boundary layer (PBL), convection, and radiation. We have demonstrated that the results of our efforts have improved forecasts of temperature, wind, and humidity. The improvement in prediction of these meteorological variables supports our long term goal to produce more accurate cloud forecasts.

2. DESCRIPTION OF THE PL GSM

In concert with the development of an improved radiative transfer parameterization, we have developed a state-of-the-art GSM. The adiabatic portion of the model was originally acquired from the National Meteorological Center (NMC) through Sela.[1] This portion of the model was completely rewritten and the hydrodynamics reformulated as reported by Brenner et al.[2,3] A normal mode initialization scheme developed by Ballish[4] was also acquired from NMC at that time and installed for use at PL. To the adiabatic model acquired from NMC, we added the Oregon State University planetary boundary layer,[5,6] the University of Maryland gravity wave drag,[7] the University of Utah radiative transfer,[8] and the European

[1]Sela, J. (1980) Spectral Modeling at the National Meteorological Center, *Mon. Wea. Rev.*, 108: 1279-1292.

[2]Brenner, S., Yang, C.-H., and Mitchell, K. (1984) *The AFGL Spectral Model: Expanded Resolution Baseline Version*, AFGL-TR-84-0308, Air Force Geophysics Laboratory, Hanscom AFB, MA. [NTIS ADA 160370]

[3]Brenner, S., Yang, C.-H., and Yee, S.Y.K. (1982) *The AFGL Spectral Model of the Moist Global Atmosphere: Documentation of the Baseline Version*, AFGL-TR-82-0393, Air Force Geophysics Laboratory, Hanscom AFB, MA [NTIS ADA 129283]

[4]Ballish, B.A. (1980) *Initialization Theory and Application to the NMC Spectral Model*, Ph.D. Thesis, Dept of Meteorology, University of Maryland.

[5]Mahrt, L., Pan, H.-L., Paumier J., and Troen, I. (1984) *A Boundary Layer Parameterization for a General Circulation Model*, AFGL-TR-84-0063, Air Force Geophysics Laboratory, Hanscom AFB, MA. [NTIS ADA 144224]

[6]Mahrt, L., Pan, H.L., Ruscher, P., Chu, C.-T., and Mitchell, K. (1987) *Boundary Layer Parameterization for a Global Spectral Model*, AFGL-TR-87-0246, Air Force Geophysics Laboratory, Hanscom AFB, MA. [NTIS ADA 199440]

[7]Pierrehumbert, R.T. (1987) An essay on the parameterization of orographic gravity wave drag, Seminar/Workshop on Observation, theory and modeling of orographic effects, 15-20 September 1986, European Center for Medium-Range Weather Forecasts, Shinfield Park, Reading, U.K., Vol 2, 251-282.

[8]Ou, S.-C., Liou, K.-N. (1988) *Development of Radiation and Cloud Parameterization Programs for AFGL Global Models*, AFGL-TR-88-0018, Air Force Geophysics Laboratory, Hanscom AFB, MA. [NTIS ADA 193369]

Center for Medium-range Weather Forecasting moist convection[9] parameterizations. We sponsored the University research leading to all but the moist convection parameterization. Figure 1 shows the relationship between the adiabatic portion of our model, the parameterization packages, and the functioning of the overall model. Each depicted module modifies the variables in parentheses. We will refer hereafter to this configuration of the model as PL-91.
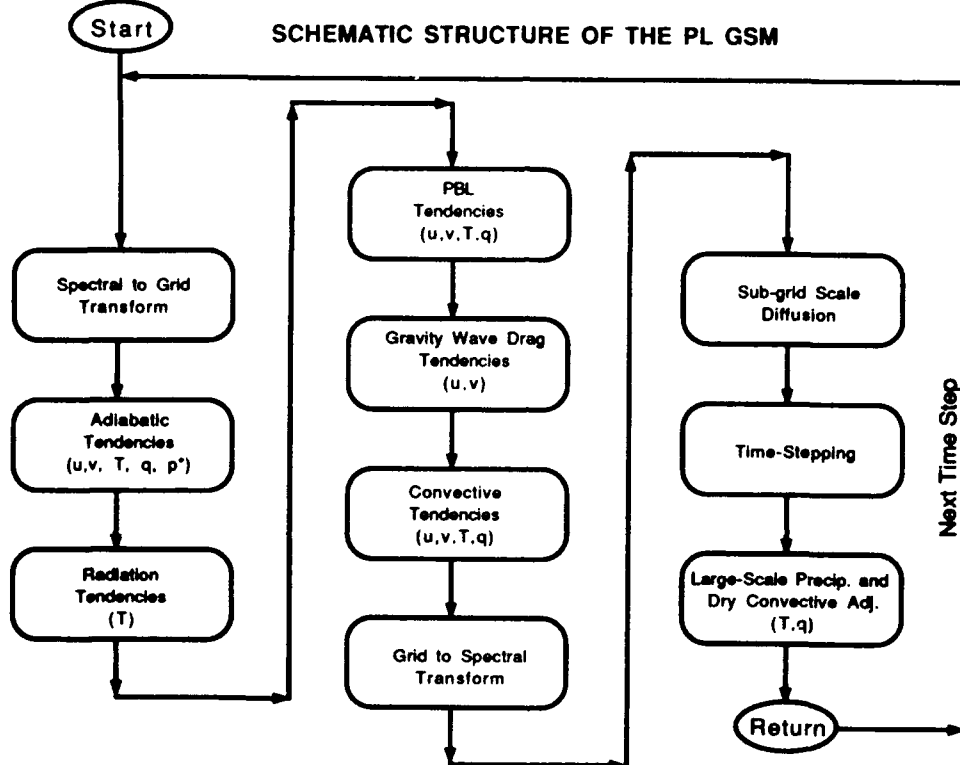

Figure 1. Key Functions of the PL GSM

3. RADIATION PARAMETERIZATION DESCRIPTION

3.1 Clear-Sky Formulation

The University of Utah parameterization employs a broad band approach to

[9]Tiedtke, M. (1989) A Comprehensive Mass Flux Scheme for Cumulus Parameterization in Large-Scale Models, *Mon. Wea. Rev.*, **117**, 1779-1800.

radiative transfer by dividing the long and shortwave portions of the electromagnetic spectrum into 5 and 25 bands respectively. The radiation parameterization performs both the long and shortwave flux calculations every 3 hours and at every other model grid point in both latitude and longitude. The resulting tendencies are imposed on the grid point and its neighbor at every time step during the three-hour period. This method results in a significant savings in computation time. The Utah radiation scheme includes absorption by water vapor, carbon dioxide, and ozone. The radiation code uses the model-predicted water vapor specific humidity, and specified monthly climatological values of ozone mixing ratio that vary in latitude and altitude.[10] A single invariant value of carbon dioxide mixing ratio is also prescribed. For each gaseous specie, the Utah parameterization calculates an upward and downward clear-sky flux at the interfaces of each model layer. The model determines the net flux at each model layer interface from the upward and downward flux components at the interface. The divergence of the net flux (difference between the net flux at the top and bottom of the model layer) determines the model layer's cooling rate. These processes are illustrated schematically in Figures 2 and 3 (for short and longwave aspects respectively) for both clear and cloudy sky conditions.

3.2 Cloudy-Sky Formulation

In addition to the clear sky calculation, the Utah scheme allows for the presence of cloud in up to three cloud-forming regions or decks. The decks are several model layers thick and correspond to high, middle, and low clouds (Figure 4). To account for cloudy and partly cloudy conditions, the radiation parameterization calculates a heating rate for a completely overcast column. If the grid box is less than overcast, the heating rates for the clear and cloudy columns are weighted by their respective fractional amounts. In PL-91, we modified the Utah parameterization to calculate

---

[10]Anderson, G., et al. Private communication.
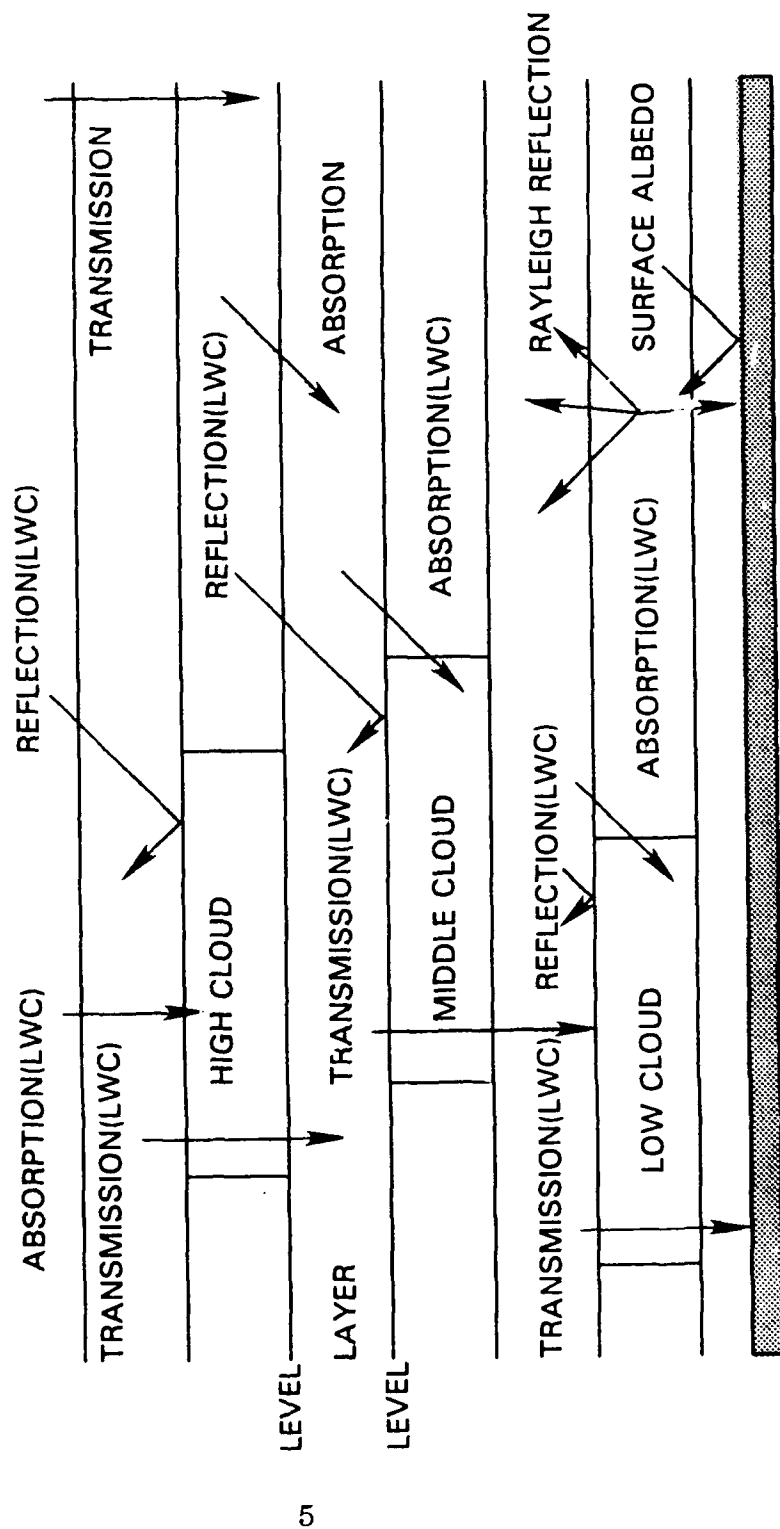
SOLAR RADIATIVE PHYSICS

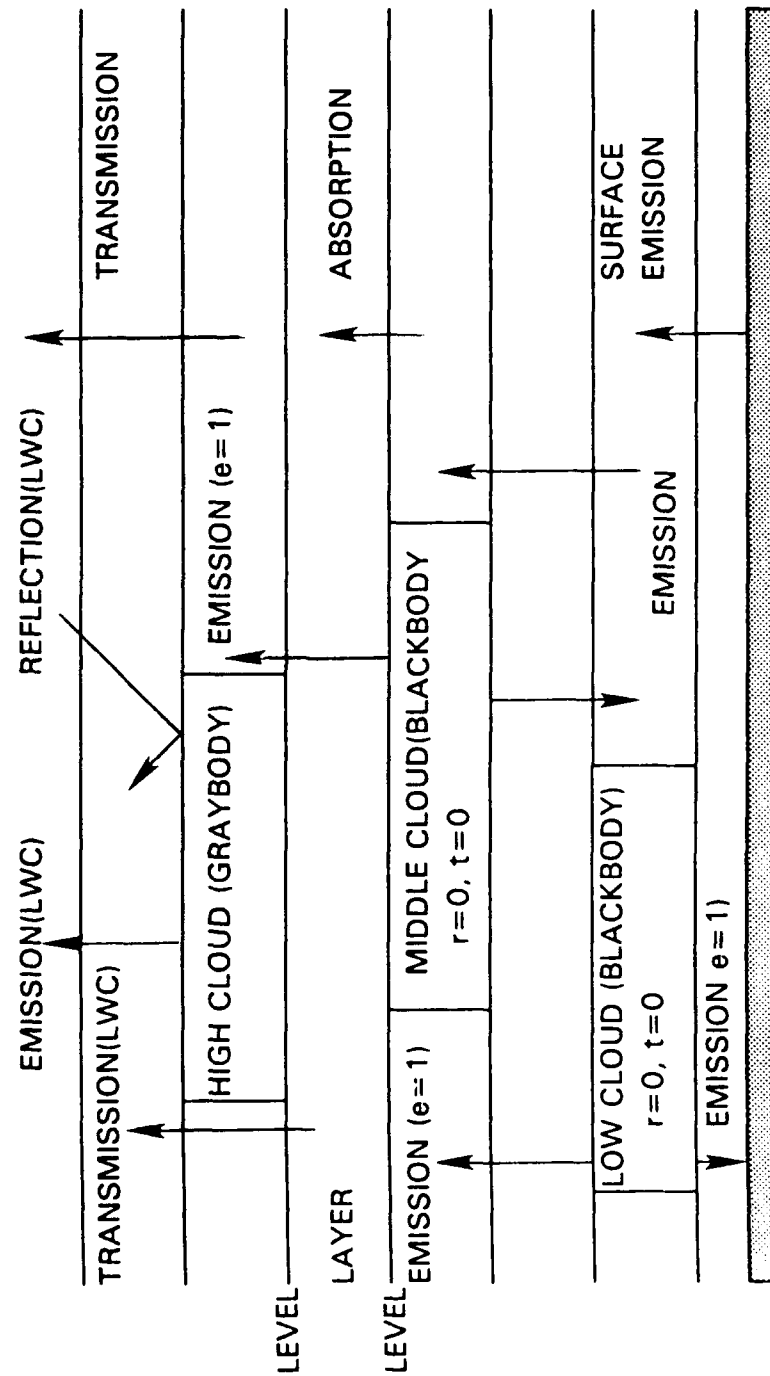
Figure 2. Solar Radiative Physics.

IR RADIATIVE PHYSICS

Figure 3. IR Radiative Physics.

6

the heating rates according to the relationship:

$$Q = \sum_{j=1}^{m} \left(\eta_j Q_{cldy_j} \right) + \left(1 - \sum_{j=1}^{m} \eta_j \right) Q_{nocld} \quad m \leq 3 \tag{1}$$

Where Q, the total heating rate, is determined by summing both the weighted cloudy heating rates Q_{cldy} and the weighted clear-sky heating rate Q_{nocld}. Q_{cldy} is determined for each of m possible radiative scenarios and weighted by the appropriate fractional cloud amount η. Figure 4 illustrates the set of radiative scenarios. The variable j ranges from 1 to 3 and is derived from model diagnosed cloud (see example below). The difference (one minus the sum of all the fractional cloud amounts) weights the fraction of the grid box considered clear.
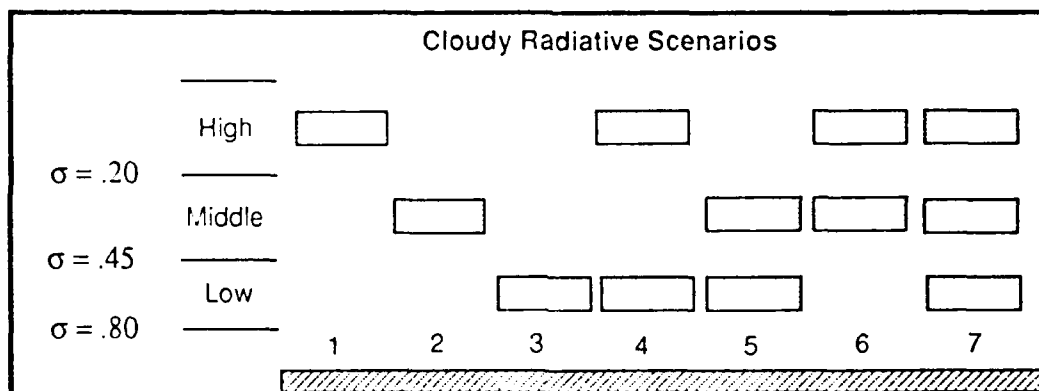
Figure 4. The set of Radiative Scenarios for Three Cloud Decks

Within each cloud deck, clouds can be either stratiform or convective. A modified version of the methodology described by Slingo[11] creates the fractional amounts of both types of clouds. We outline later (Section 4) the innovative aspects of our implementation of the Slingo scheme. After specifying the deck's cloud amount (derived from layer cloud amounts determined according to the Slingo methodology),

---

[11]Slingo, J.M. (1987) The Development and Verification of a Cloud Prediction Scheme for the ECMWF, *Q.J.R. Meteorol. Soc.*, **113**, 371-386.

the radiation parameterization positions the cloud in the layer where the sum of convective and stratiform cloud is greatest.

The parameterization combines the cloud amounts for the three cloud decks into a maximum of four radiative scenarios (three cloudy and one clear). Figure 5 shows the creation of cloudy radiative scenarios from given grid point clouds. The assumption that cloud decks overlap each other in a maximum sense leads to three cloudy scenarios. The first scenario in the example arises from the superposition of the smallest cloud amount, high, on the larger cloud amounts of the middle and low

Figure 5. Conversion from Model Diagnosed Cloud to Radiative Scenarios Assuming Maximum Overlap of Deck Clouds

decks. The next largest cloudy deck, middle, minus the overlap in scenario 1 (20%), dictates the composition of scenario two (35% of the middle cloud overlapping the low cloud). Scenario three contains the portion (25%) of the low cloud radiating directly to space. The radiative calculation benefits from the multiple radiative scenarios through an appropriate vertical distribution of cloud heating/cooling and realistic interactions between 1) two neighboring cloud decks; 2) a cloud deck and space; and, 3) a cloud deck and the model's surface. In addition to the cloudy scenarios, a "no cloud" scenario exists. For the example in Figure 5, the radiation parameterization performs the clear-sky calculation for the 20 percent of the grid box not covered by any cloud.

The description of the radiation parameterization in PL-91 above represents an

evolution away from the parameterization delivered by the University of Utah in 1988. Table 1 describes the changes we have made to the 1988 delivery. The new cloud liquid water contents reduce cloud-top cooling for the low and middle clouds and raise the warming of the high cloud. The change significantly reduced a cold bias observed in the model temperatures field. The choice of a modified Slingo scheme, which is described below, over the Geleyn[12] scheme came as a result of an overspecification of cloud in our model by the Geleyn scheme. Like the change to liquid water content, the reduction in cloud resulting from use of the modified Slingo scheme also improved the model's cold temperature bias. A final measure to reduce the model's cold bias came as we allowed the radiation code to accommodate the four radiative scenarios.

Table 1. Difference Between Utah-88 and PL-91.

ITEM	UTAH-88	PL-91
Cloud Liquid Water Content	High = 0.00336 g/kg Middle = 0.12 g/kg Low = 0.165 g/kg	High = 0.00672 g/kg Middle = 0.12 g/kg Low = 0.165 g/kg
Cloud Specification Scheme	Geleyn (RH Based)	Modified-Slingo (RH, Precipitation, Vertical Velocity, & Stability Based)
Cloud Configuration	Two Radiative Scenarios (1 Clear & 1 Cloudy) Maximum Overlap Full Deck	Four Radiative Scenarios (1 Clear & 3 Cloudy) Maximum Overlap Single Layer At Max Cloud
High Cloud Limit	$\sigma = 0.2$	$\sigma = 0.2$ tropics $\sigma = 0.25$ mid-latitude $\sigma = 0.30$ poles
Ozone Specification	Single Climatological Profile For All Cases	Interpolated Latitudinally From 10° latitude Band Averages Of Monthly Climatologies

---

[12]Geleyn, J.F. (1981) Some Diagnostics of the cloud-radiation interaction in the ECMWF forecasting model, Workshop on radiation and cloud-radiation interaction in numerical modeling, 15-17 October 1990, European Center for Medium Range Weather Forecasts, Shinfield Park, Reading, U.K.

4. CLOUD SPECIFICATION FORMULATION

4.1 The Slingo Scheme

The radiation parameterization specifies cloud for its own internal use. Therefore, we have judged the cloud forecast by its impact on the large-scale forecast fields vis-a-vis the radiation calculation. In PL-91, we used a modified version of the Slingo scheme. We constrained high cloud to form below $\sigma = 0.2$ in the tropics, $\sigma = 0.25$ in the mid-latitudes, and $\sigma = 0.30$ in the high latitudes. Middle and low cloud were not allowed to ascend above $\sigma = 0.45$ and 0.8 respectively. Finally, cloud was not allowed to form in the lowest model layer. Figure 4 shows these boundaries. The critical relative humidity, RHc, used in the low and middle cloud decks was 0.8. For high clouds, we adopted the formulation of Kiehl[13]

$$RH_C = 0.8 + 0.18 \left(\frac{(p_{mid} - p)}{(p_{mid} - p_{hi})} \right) \tag{2}$$

where p_{mid} is the sigma layer pressure corresponding to the highest layer in the middle cloud deck and p_{hi} the layer pressure of the highest layer in the high cloud deck.

Like Kiehl, we used RHc to diagnose stratiform clouds in all layers regardless of the presence or absence of convective cloud. We departed from the Slingo scheme by abandoning the convective cirrus computation and ignoring the environmental relative humidity formulation. A final departure from the Slingo scheme is the use of 100 percent, 50 percent, and 25 percent of diagnosed convective cloud cover in the low, middle, and high cloud decks, respectively. We use the remainder of the provisions of the Slingo algorithm as described in her 1987 paper.

---

[13]Kiehl, J.T. (1991) Modeling and Validation of Clouds and Radiation in the NCAR Community Climate Model, *ECMWF/WCRP Workshop: Clouds, Radiation Transfer and the Hydrological Cycle*, 249-272.

4.2 The Cloud Forecast

The clouds produced by PL-91 are in general agreement with the Henderson-Sellers[14] and the International Satellite Cloud Climatology Project (ISCCP)[15] cloud climatologies. Figure 6 shows a January zonal average of model-produced total cloud and the climatologies. We created the model cloud by averaging clouds from three 10-day forecasts initialized from the FGGE-3B analysis of 2, 12, and 22 January 1979 at 1200 UTC. We averaged clouds, diagnosed every 18 hours in each of the three 10-day periods, over all diagnosed times, and zonally-averaged these results. In all curves, the minima in the cloud field near 30° N and 30° S mark the descending branches of the Hadley circulation. The maximum in cloud cover corresponding to the Intertropical Convergence Zone (ITCZ) is also present in all curves. However, the
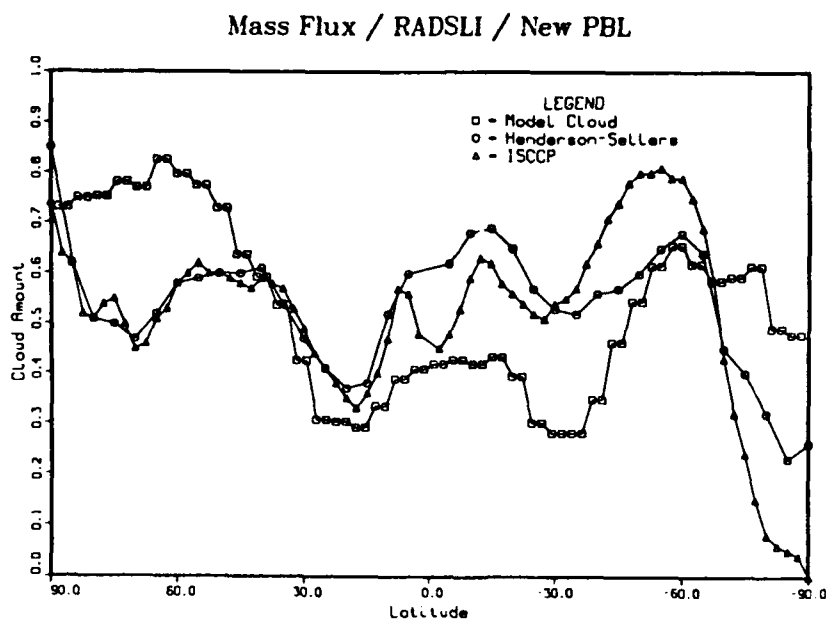

PL-91 (Jan)

Mass Flux / RADSLI / New PBL

Figure 6.   Total Cloud from PL-91, and the ISCCP15 and Henderson-Sellers Climatologies.

---

[14]Henderson-Sellers, A. (1986) Layer Cloud Amounts for January 1979 from 3D-Nephanalysis, *Journal of Climate and Applied Meteorology,* **25**, 118-132.

[15]Rossow, W.B., and Schiffer, R.A. (1991) ISCCP Cloud Data Products, *Bulletin of the American Meteorological Society,* **72**, 2-20.

11

model-produced clouds underestimate the magnitude of this topical maximum by as much as 25 percent near 15° S. A comparison between high, middle, and low cloud amounts produced by PL-91 (Figure 7a) and those shown by Henderson-Sellers (Figure 7b) indicates the underforecasting of total cloud by the model is due to insufficient middle and low clouds. In an illustration of the components of the Slingo scheme (Figure 8a-d) for day 5 of a simulation initialized at 1200 UTC on 12 January 1979, it is shown that only convective cloud (Figure 8c) contributes significantly in the tropics. Figure 10a shows the geographical distribution of this cloud component in the low deck. It appears that this cloud component forms mainly over ocean. Slingo's base stratiform cloud (Figure 8a), deduced solely from a relationship using a critical RH value, produces little cloud in the tropics. The implication is that throughout the tropics the value of RH is generally less than 80 percent in the middle and low cloud decks. In the extratropics, however, the amount of Slingo's base stratiform cloud is substantial. The cloud in Figure 8b shows Slingo's modified version of Figure 8a in which she reduces the amount of low cloud in the presence of downward vertical velocity. The reduction of stratiform cloud after accounting for subsidence is impressive. Cloud amounts are 30-40 percent less north of 40° N and south of 40° S. Clearly, a large number of grid points have downward vertical velocity. Although the Slingo scheme's inversion-based stratiform cloud (Figure 8d) forms a significant amount of low cloud, the cloud is predominantly north of 40° N in the winter hemisphere. Slingo[11] indicates that regions off the western coasts of continents are also preferred sites for the formation of large sheets of this cloud type. Figure 10b, however, shows little if any cloud off the west coasts of North America, South America, or Africa. Model cloud also deviates from the climatologies poleward of 45° N and 65° S where too much total cloud is created. While Figure 9a indicates that model high cloud is generally greater than 50 percent in the Northern Hemisphere north of 45° N, the Henderson-Sellers climatology shows high cloud cover less than 15 percent. The overproduction of high cloud is a manifestation of excess moisture in the upper part of the model atmosphere. Figure 11 represents the zonally-averaged RH difference between the day 5 forecast (valid 17 January 1979,

12

1200 UTC) and the verifying analysis (FGGE-3B). A clear moist bias exists above 35 kPa. The underproduction of low cloud (Figures 8b and 9c) especially in the tropics, is probably a result of the dry bias below 80 kPa. The GSM appears to be drying the low levels and moistening the high levels with respect to the verifying analysis.
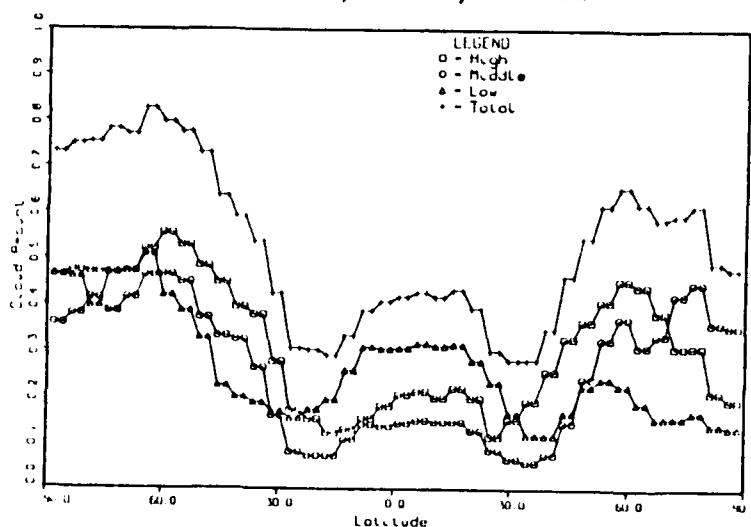
PL-91 (Jan)

Mass Flux / RADSLI / New PBL

Figure 7A. PL-91 Zonal Average High, Middle, Low and Total Cloud Amounts from Three 10-Day Forecasts Initialized from the FGGE-3B Analysis of 2, 12, and 22 January 1979 at 1200 UTC.
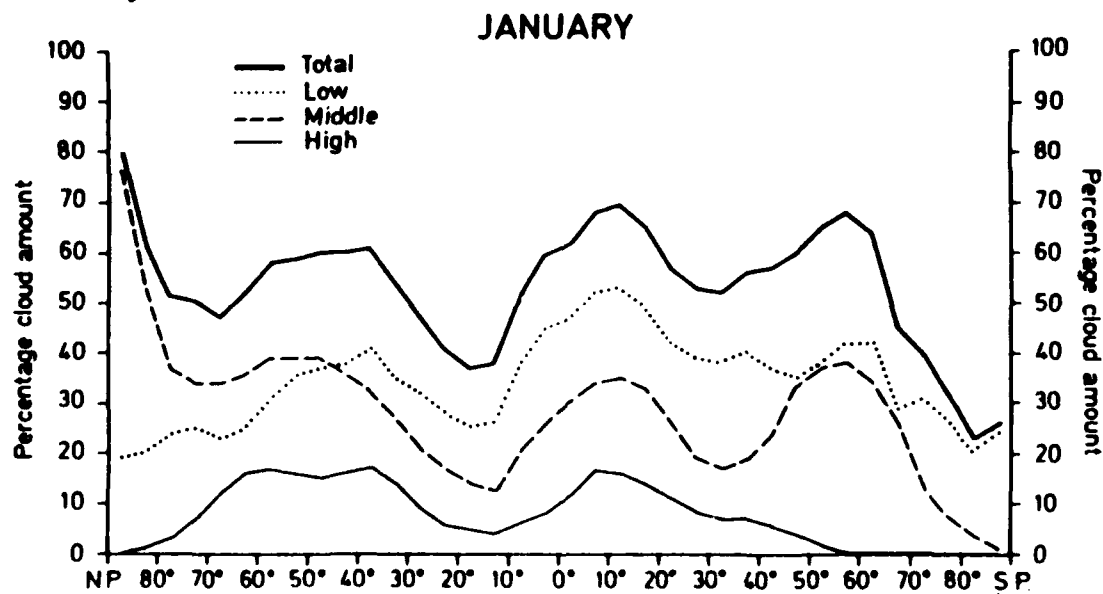

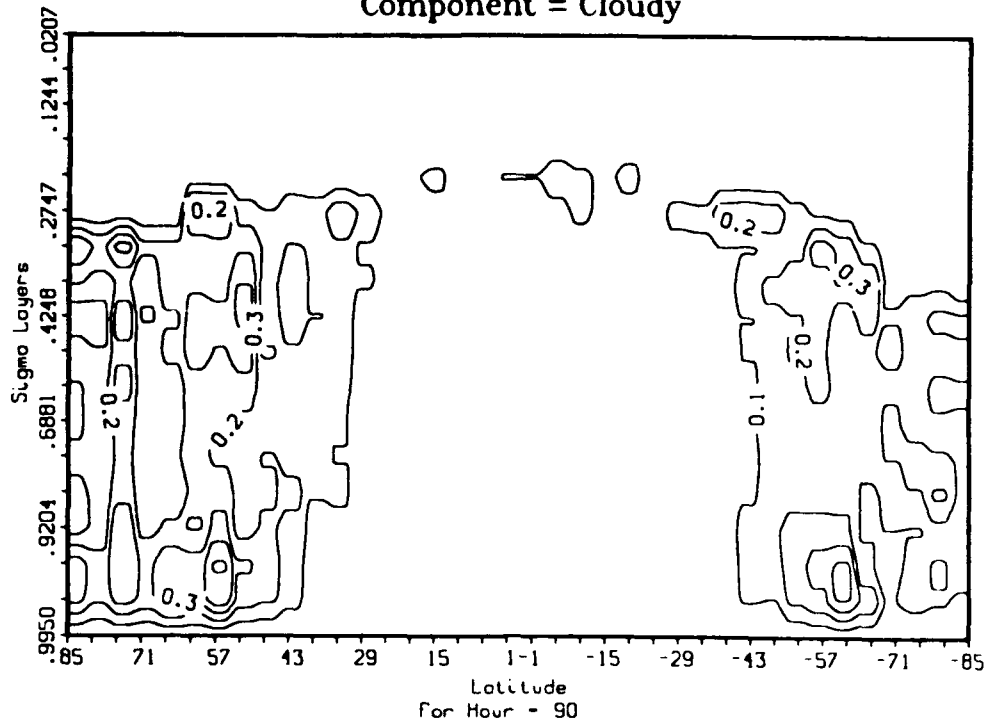Figure 7b. High, Middle, Low and Total Cloud from the Henderson-Sellers Cloud Climatology.

13

Figure 8a. Zonal Average of Slingo's Base Stratiform Cloud for Day 5 of a Forecast Initialized at 1200 UTC on 12 January 1979.

Figure 8b. Same as 8a Except for Slingo's Modified Stratiform Cloud.

14

PL-91 (12 Jan)
Mass Flux / RADSLI / New PBL
25%/75% Convective Cloud
Component = Cloudy
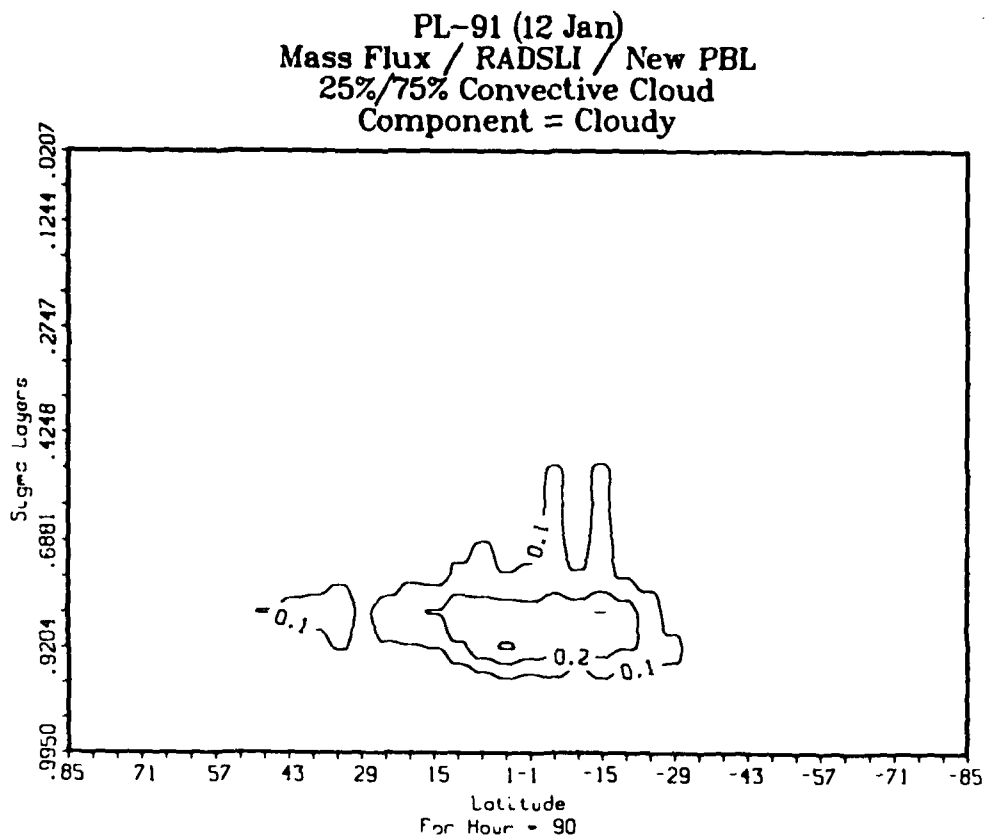
Figure 8c. Same as 8a Except for Slingo's Convective Cloud.

PL-91 (12 Jan)
Mass Flux / RADSLI / New PBL
PBL (Subtropical Stratus)
Component = Cloudy
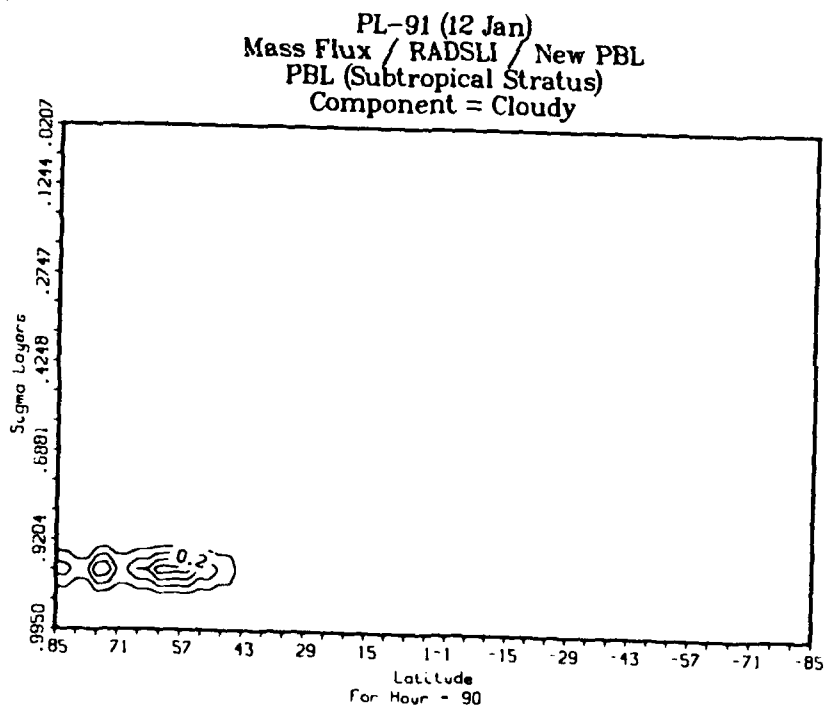
Figure 8d. Same as 8a Except for Slingo's Inversion Based Cloud.

15
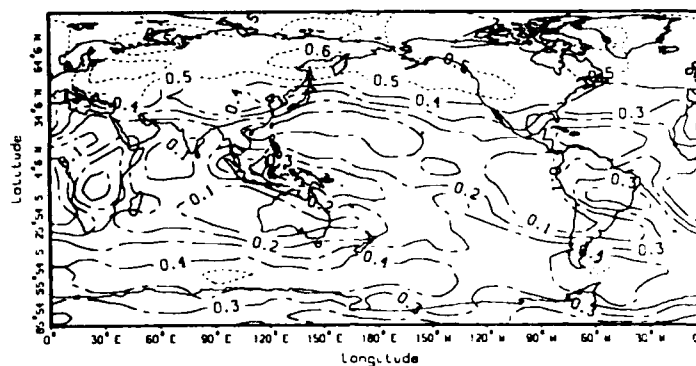
Figure 9a. Geographical Distribution of High Cloud for Model Average from Three 10-Day Forecasts Initialized from the FGGE-3B Analysis of 2, 12, and 22 January 1979 at 1200 UTC.
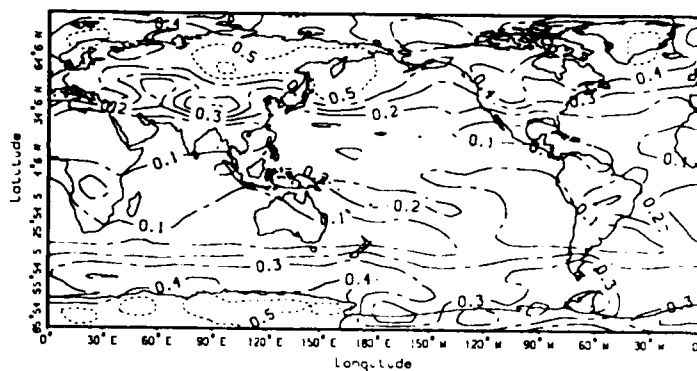
Figure 9b. Same as 9a Except for Middle Cloud.
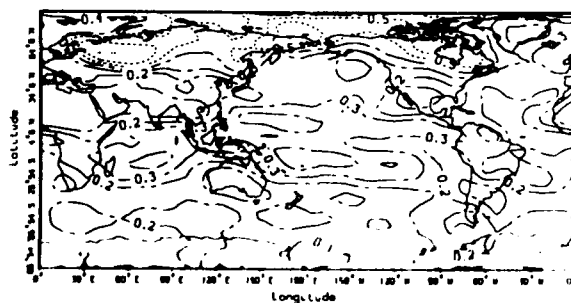
Figure 9c. Same as 9a Except for Low Cloud.

16

PL-91 (12 Jan)
Mass Flux / RADSLI / New PBL
25%/75% Convective Cloud (Low)
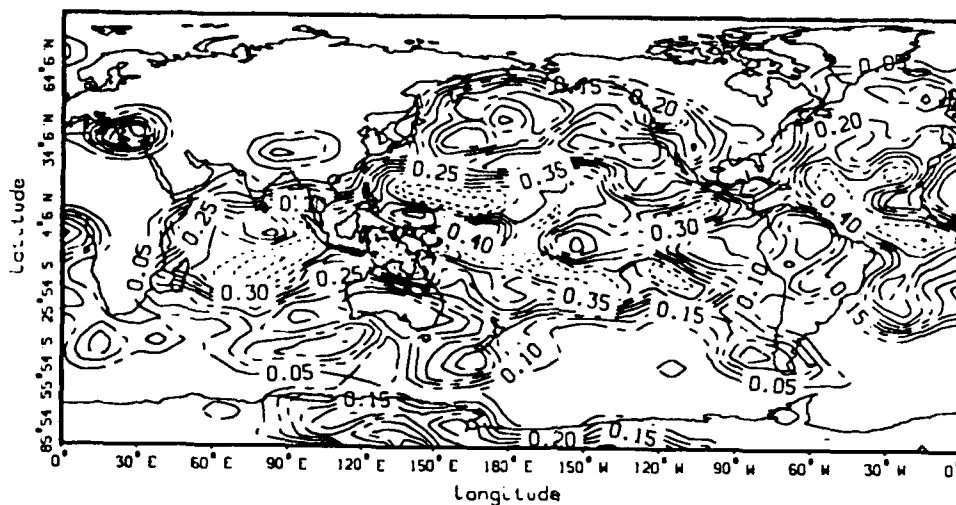
For Hour - 90

Figure 10a. Geographical Distribution of Convective Low Cloud for Day 5 of a
Forecast Initialized at 1200 UTC on 12 January 1979.

PL-91 (12 Jan)
Mass Flux / RADSLI / New PBL
PBL/Subtropical Stratus (Low)

For Hour - 90

Figure 10b. Same as 10a Except for Inversion Based Cloud.

17
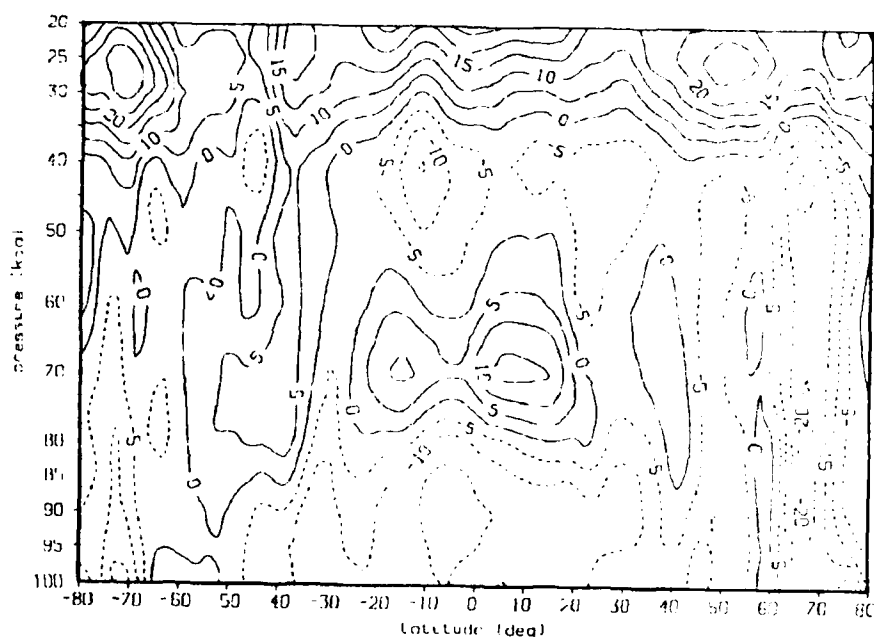
Figure 11. PL-91 Relative Humidity Error (Percent) for Day 5 of a Forecast
Initialized at 1200 UTC on 12 January 1979.

is a manifestation of excess moisture in the upper part of the model atmosphere.
Figure 11 represents the zonally-averaged RH difference between the day 5 forecast
(valid 17 January 1979, 1200 UTC) and the verifying analysis (FGGE-3B). A clear
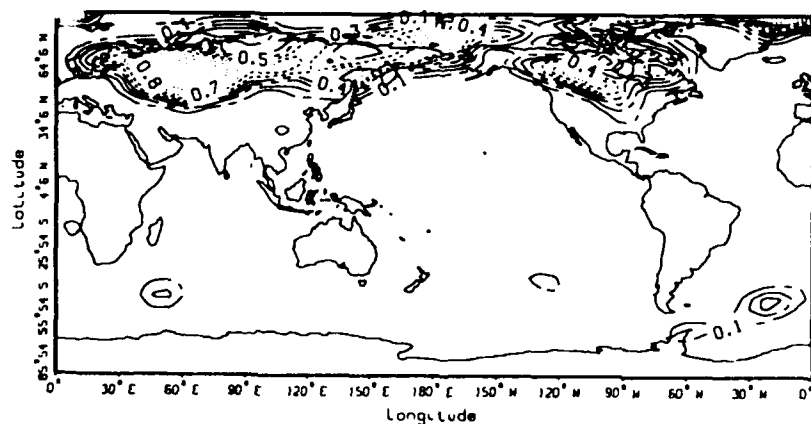moist bias exists above 35 kPa. The underproduction of low cloud (Figures 8b and 9c),
especially in the tropics, is probably a result of the dry bias below 80 kPa. The GSM
appears to be drying the low levels and moistening the high levels with respect to the
verifying analysis.

5. RADIATIVE PARAMETERIZATION PERFORMANCE

5.1 Heating Rates

The radiation parameterization furnishes, as its primary output to the forecast
model, temperature tendencies (heating rates). Figure 12 shows a zonal average of

the clear-sky heating rates. The plot shows that in the absence of clouds, radiative processes cool most of the atmosphere. Within the troposphere, water vapor accounts for the cooling. It is not surprising that the location of the highest concentration of water vapor, near the surface in the tropics, corresponds to the maximum in the
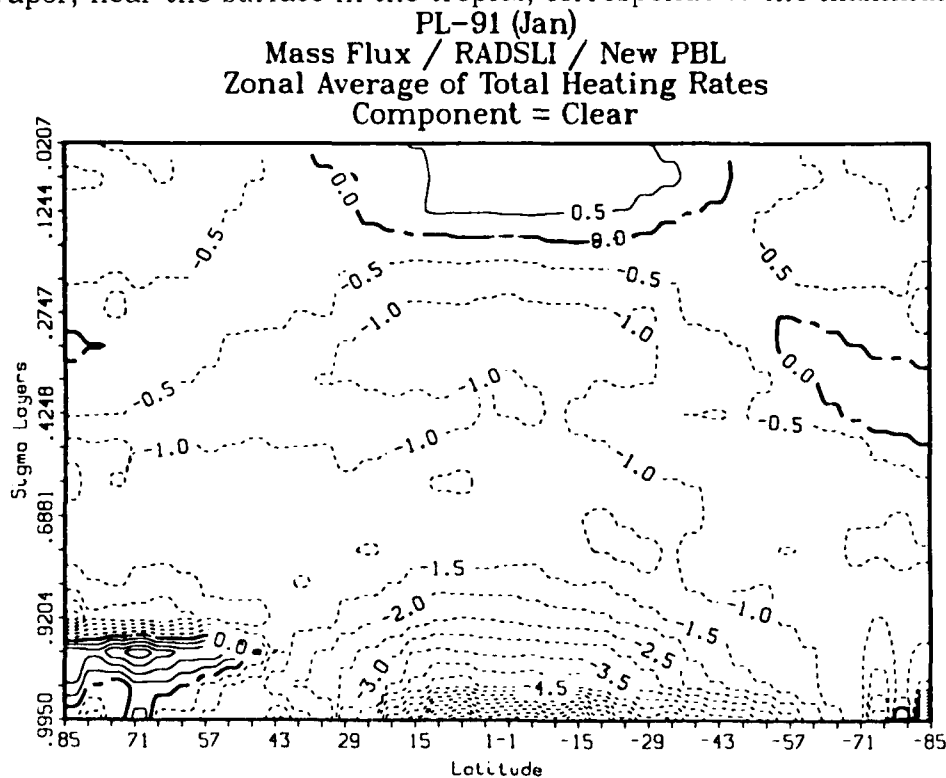
Figure 12. Zonal Average of PL-91 Generated Clear-Sky Heating Rates (°K/Day*10) from Three 10-Day Forecasts Initialized from the FGGE-3B Analysis of 2, 12, and 22 January 1979 at 1200 UTC.

cooling rates in Figure 12. The warming observed in the figure at $\sigma = 0.075$ in the tropics and $\sigma = 0.375$ in the high latitudes results from long-wave absorption by CO_2 at the tropopause. We attribute the warming north of 55° N near the surface to a strong inversion at $\sigma = 0.9204$ with the warm air radiating into the three model layers below.

In addition to clear-sky radiative effects, our model accounts for the presence of cloud. Figure 13 illustrates the impact of clouds on heating rates by subtracting clear-sky heating rates from total (that is, including cloud) heating rates. It is

apparent by comparing Figure 13 with Figure 12 that clouds both enhance and mitigate the clear-sky cooling. The enhanced cooling outside the tropics and above σ = 0.4248 arises from cloud top cooling of high cloud. Cloud top cooling also produces the area of increased cooling in the tropics above σ = 0.856. In this case, low cloud contributes to the cooling. In addition to cloud top cooling, cloud base warming impacts the clear-sky heating rates. Cloud base warming manifests itself in the tropics below σ = 0.856 where there is significant low cloud. Interestingly, clouds forming north of 45° N near σ = 0.860 provides significant cooling in the same layer where warming occurred in Figure 12. The Slingo scheme, forming cloud at the base of the inversion that warmed the third model layer in Figure 12, act to offset the inversion warming by imposing cloud-top cooling.
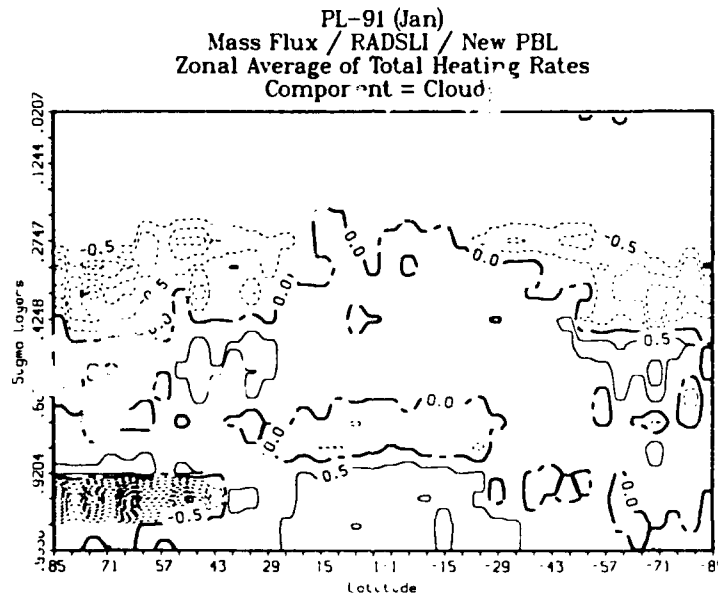

Figure 13. Zonal Average of PL-91 Generated Cloud Forced Heating Rates (°K/Day*10) from Three 10-Day Forecasts Initialized from the FGGE-3B Analysis of 2, 12, and 22 January 1979 at 1200 UTC.

5.2   Outgoing Longwave Radiation

An appropriate means of verifying profiles of the zonally-averaged heating rates shown in Figures 12 and 13 does not exist. Therefore, we decided to evaluate our

radiation scheme using fluxes at the top of the atmosphere (TOA). We found that model fluxes at the TOA generally agreed with satellite-derived fluxes from the Earth Radiation Budget Experiment (ERBE).[16] Figure 14 depicts the zonal average of model and ERBE outgoing longwave radiation (OLR) for the clear-sky case in January. In this case, the ERBE data comes from 1986. An evaluation of the variability of the global average of OLR for the seven Januaries (Table 2) from 1979 to 1985 reveals a standard deviation of 0.5 W/m^2. Therefore, the comparison of 1979 model results with the 1986 ERBE data seems reasonable. The clear bias towards lower values of OLR in the tropics is unmistakable. The 10-20 W/m^2 difference between model and ERBE clear-sky OLR equates to a surface temperature difference

Table 2. Global Averages Of OLR (W/m^2) For January 1979 - 1985

Year	Jan 79	Jan 80	Jan 81	Jan 82	Jan 83	Jan 84	Jan 85
Global OLR	231.073	231.923	232.105	230.944	231.515	230.823	230.020

of 2-4 °C. The latitudes over which the difference is greatest corresponds to the latitudes with the greatest amount of ocean. Perhaps the sea surface temperatures used by the model are too low.

In addition to evaluating the zonal average of OLR, we have looked at the geographical distribution of OLR. Figure 15a shows our model's monthly average of geographical distribution of OLR at the TOA for January 1979. Figure 15b shows the corresponding ERBE observations. In Figure 15a, the convectively active regions over South America and Africa, with their high cloud tops, show OLR values as low as 220 and 230 W/m^2 respectively. Figure 10a shows the maxima in the high cloud located in these geographical areas. The agreement between the locations of the OLR minima is good. However, the magnitudes of the model minima are 30 W/m^2 higher than the

---

[16]Bess, T.D., and Smith, G.L. (1987) *Atlas of Wide-Field-of-View Outgoing Longwave Radiation Derived from Nimbus & Earth Radiation Budget Data Set - November 1978 to October 1985, NASA Reference Publication 1186*, NASA Langley Research Center, Hampton, VA, p 11.

PL-91 (Jan)

Mass Flux / RADSLI / New PBL

Figure 14. PL-91 TOA Clear-Sky Outgoing Longwave Radiation (W/m^2) from three 10-day forecasts initialized from the FGGE-3B analysis of 2, 12, and 22 January 1979 at 1200 UTC.

PL-91 (Jan)
Mass Flux / RADSLI / New PBL
Net IR Flux at TOA
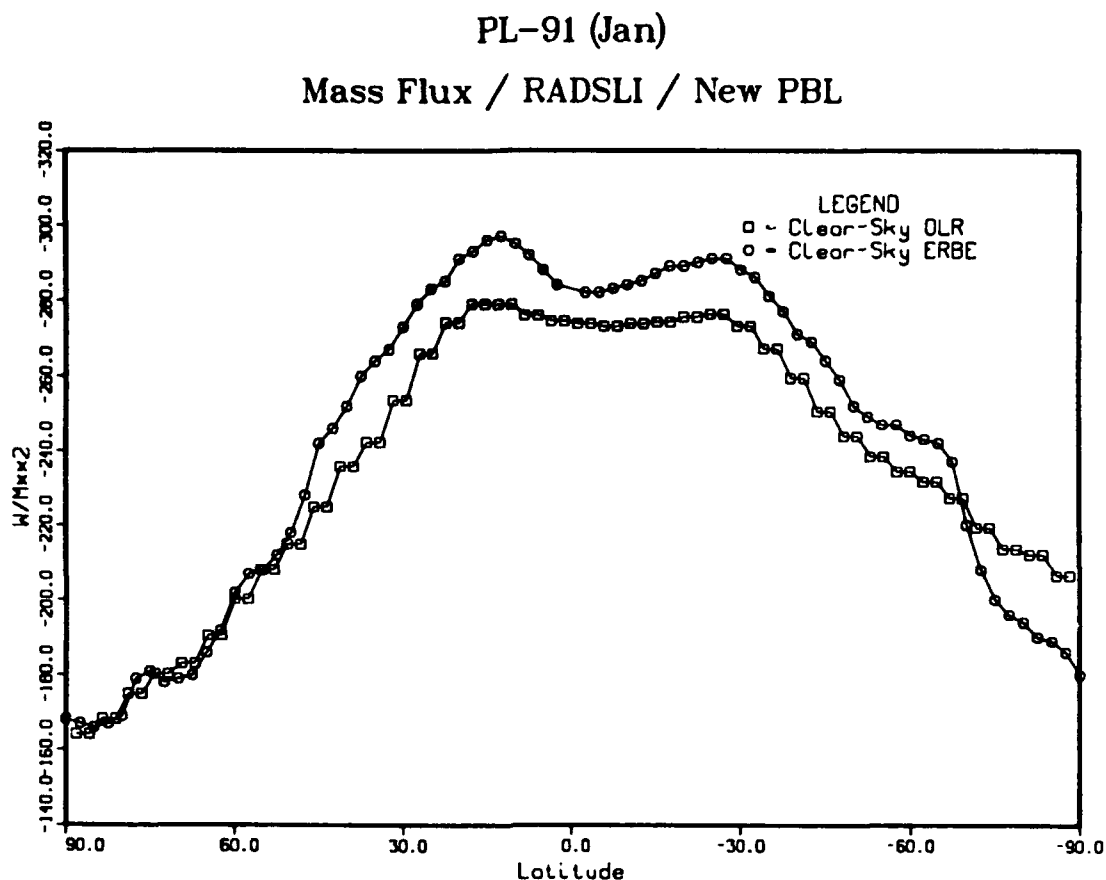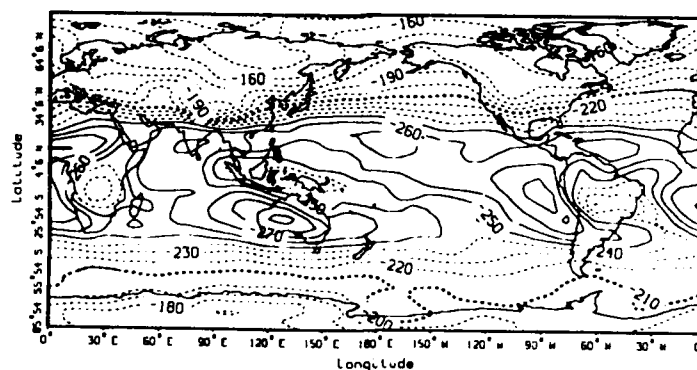

Figure 15a. PL-91 TOA Outgoing Longwave Radiation (W/m^2) from Three 10-Day Forecasts Initialized from the FGGE-3B Analysis of 2, 12, and 22 January 1979 at 1200 UTC.
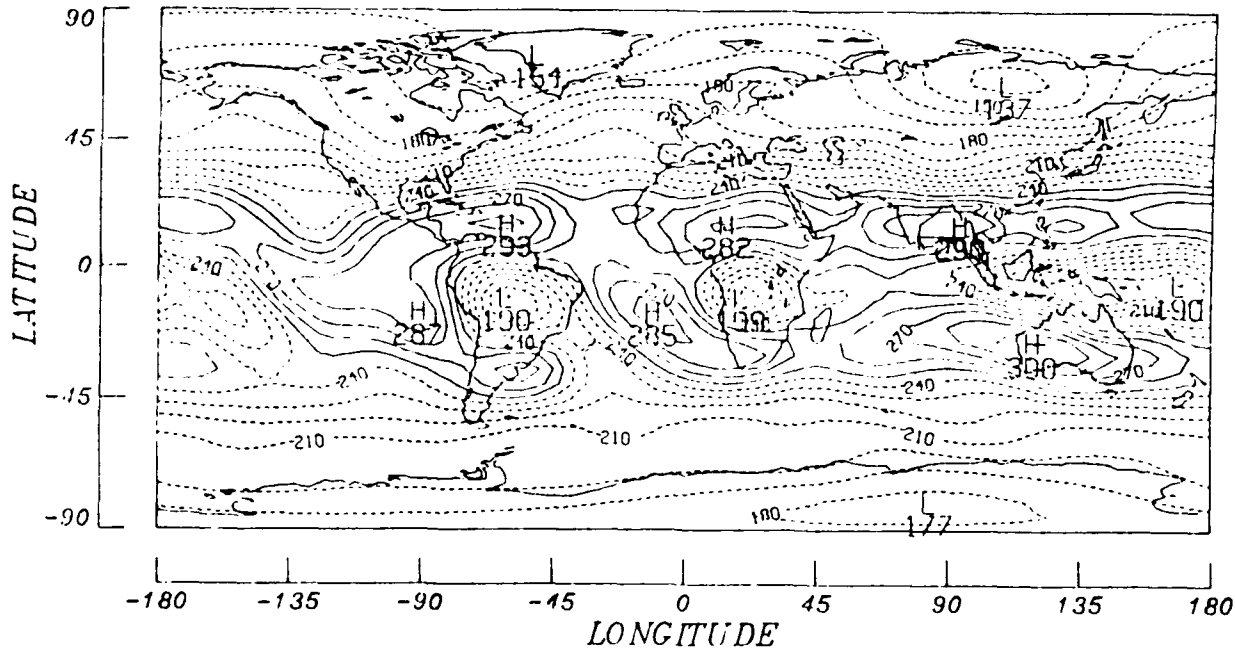
22

Figure 15b. January 1979 TOA Outgoing Longwave Radiation (W/m²) for ERBE.[16]

ERBE values. The model exhibits a still larger error in magnitude of over 40 W/m² in the western Pacific near New Guinea. The higher OLR minimum in the convectively active regions is due either to the insufficient generation of convective cloud in the model, or convective cloud tops that are too warm (too low), or both. The latter possibility could result in part from the imposition of σ = 0.2 as a limit on cloud tops in the tropics. This was done to reduce the model's moist bias (and its effect on forming high stratiform cloud) occurring in model layers above σ = 0.2.

Regions of relatively clear skies like Western Australia and Central Africa show maxima in OLR. Model and ERBE OLR values agree well in these clear sky areas over land. The differences in OLR values are less than 5 W/m.² Clear-sky regions over oceans, however, show significant deviations. To the north and west of South America for example, a large area of 280 W/m² is missing. This may be explained in part by the lower than expected model produced clear-sky OLR seen in Figure 12. Cooler sea-surface temperatures would account for both errors. In the Caribbean, the difference between model and observed OLR is about 20 W/m². This departure corresponds to a blackbody temperature difference of 4.5° K - about the same as

23

6. SUMMARY

Given our goal to develop a cloud-radiation parameterization capable of simulating IR and solar radiative transfer within a GSM, we can point to the successful simulation of observed satellite-derived OLR values. The parameterization positions the maxima and minima in the OLR field correctly. The correct spatial representation of OLR implies the model is accurately locating clouds. The zonal average of cloud cover shows similar features when compared to two cloud climatologies. Given model specified clouds, the radiation code produces reasonable zonal averages of heating rates. We believe the heating rates to be acceptable in light of their impact on the model's temperature field. The model also simulates the expected cloud-top cooling and cloud-bottom warming.

7. CONCLUSIONS AND RECOMMENDATIONS

Further research must identify and correct the cause of bias in the tropical clear-sky OLR towards values that are too low. One possible area of investigation involves the effect of increased model resolution. Increased resolution may mitigate some of the bias by enhancing the downward vertical velocity in the descending branch of the Hadley cell. The subsidence would act to dry out the air and raise the OLR. Another avenue to consider involves the evaluation of the model's sensitivity to prescribed sea surface temperature. One possible sensitivity study involves interpolating between the existing 12 monthly sea-surface temperature fields, to create intermediate sea-surface temperature fields. An experiment could then be conducted by applying the appropriate sea-surface temperature field to the appropriate 1/3 of the month.

Having ensured the veracity of the clear-sky calculation, the next step would be to improve model-specified cloud. Future research should isolate the cause and correct the apparent drying at low and moistening at high levels. The moistening at high levels is responsible for the overforecasting of high cloud in the extratropics. An

investigation of cloud specification should also look at the production of shallow convection as a source of excessive low cloud in what are cloud-free areas in the subtropics. Another issue related to convection requiring further study is the identification of the cause of the overestimate of OLR in convectively active regions. Attention should be paid to the height and amount of convective high cloud.

In addition to temperature tendencies provided to the parent model, the radiation code provides the planetary boundary layer parameterization (PBL) downward solar and IR fluxes. The diurnal cycle in this input is currently limited to eight times a day. Ideally, the PBL should receive independently calculated fluxes each time step. The solar code is computationally inexpensive. This portion of the radiation code could be called at each time step. The IR calculation can be simulated at intermediate time steps, at the surface, using a σT^4 approximation.

References

1.   Sela, J. (1980) Spectral Modeling at the National Meteorological Center, *Mon. Wea. Rev.*, **108**: 1279-1292.

2.   Brenner, S., Yang, C.-H., and Yee, S.Y.K. (1982) *The AFGL Spectral Model of the Moist Global Atmosphere: Documentation of the Baseline Version,* AFGL-TR-82-0393, Air Force Geophysics Laboratory, Hanscom AFB, MA. [NTIS ADA 129283]

3.   Brenner, S., Yang, C.-H., and Mitchell, K. (1984) *The AFGL Spectral Model: Expanded Resolution Baseline Version,* AFGL-TR-84-0308, Air Force Geophysics Laboratory, Hanscom AFB, MA. [NTIS ADA 160370]

4.   Ballish, B.A. (1980) *Initialization Theory and Application to the NMC Spectral Model,* Ph.D. Thesis, Dept. Of Meteorology, University of Maryland.

5.   Mahrt, L., Pan, H.-L., Paumier, J., and Troen, I. (1984) *A Boundary Layer Parameterization for a General Circulation Model,* AFGL-TR-84-0063, Air Force Geophysics Laboratory, Hanscom AFB, MA. [NTIS ADA 144224]

6.   Mahrt, L., Pan, H.-L., Ruscher, P., Chu, C.-T. and Mitchell, K. (1987) *Boundary Layer Parameterization for a Global Spectral Model,* AFGL-TR-87-0246, Air Force Geophysics Laboratory, Hanscom AFB, MA. [NTIS ADA 199440]

7.   Pierrehumbert, R.T. (1987) An essay on the parameterization of orographic gravity wave drag, Seminar/Workshop on Observation, Theory and Modeling of Orographic Effects, 15-20 September 1986, European Center for Medium-Range Weather Forecasts, Shinfield Park, Reading, U.K., Vol. 2, 251-282.

8.   Ou, S.-C., Liou, K.-N. (1988) Development of Radiation and Cloud Parameterization Programs for AFGL Global Models, AFGL-TR-88-0018, Air Force Geophysics Laboratory, Hanscom AFB, MA. [NTIS ADA 193369]

9.   Tiedtke, M. (1989)   A Comprehensive Mass Flux Scheme for Cumulus Parameterization in Large-Scale Models, *Mon. Wea. Rev.*, **117,** 1779-1800.

10. Anderson, G., et al.   Private Communication.

11. Slingo, J. M. (1987) The Development and Verification of a Cloud Prediction Scheme for the ECMWF, *Q. J. R. Meteorol. Soc.*, **113,** 371-386.

12. Geleyn, J. F. (1981) Some diagnostics of the cloud-radiation interaction in the ECMWF forecasting model, Workshop on Radiation and Cloud-radiation Interaction in Numerical Modeling, 15-17 October 1990, European Center for Medium-Range Weather Forecasts, Shinfield Park, Reading, U.K.

13. Kiehl, J. T. (1991) Modeling and Validation of Clouds and Radiation in the NCAR Community Climate Model, *ECMWF/WCRP Workshop: Clouds. Radiation Transfer and the Hydrological Cycle,* 249-272.

14. Henderson-Sellers, A. (1986) Layer Cloud Amounts for January 1979 from 3D-Nephanalysis, *Journal of Climate and Applied Meteorology,* **25,** 118-132.

15. Rossow, W. B., and Schiffer, R. A. (1991) ISCCP Cloud Data Products, *Bulletin of the American Meteorological Society,* **72,** 2-20.

16. Bess, T.D., and Smith, G.L. (1987) Atlas of Wide-Field-of-View Outgoing Longwave Radiation Derived From Nimbus 7 Earth Radiation Budget Data Set - November 1978 to October 1985, NASA Reference Publication 1186, NASA Langley Research Center, Hampton, VA, p 11.